Aeroacoustics Conferences
26-29 May 2026, Brussels, Belgium
32nd AIAA/CEAS Aeroacoustics Conference (2026)

10.2514/6.2026-3532

Numerical Study of Self-Sustained Aeroacoustic Modes in a Quasi-Axisymmetric Cavity

Frits de Prenter*and Damiano Casalino†

TU Delft, Kluyverweg 1, 2629 HS Delft, The Netherlands

In this contribution, we numerically study an aeroacoustic instability in deep quasi-axisymmetric cavities. An experimental study by Faure-Beaulieu et al. (2023) shows that a deep axisymmetric cavity in a pipe flow can cause a constructive hydrodynamic-acoustic feedback, in which multiple regimes can be observed. In this study, we numerically replicate these regimes and investigate the effect of geometrical imperfections that break the axisymmetry of the setup.

I. Nomenclature

l_s, l_t, W, R, r	=	geometry parameters (as in Fig. 1)
α	=	symmetry parameter
J_1	=	Bessel function of the first kind
p	=	pressure
t	=	time
ω	=	frequency
A	=	amplitude (as in Eq. (1))
χ	=	nature angle (as in Eq. (1))
θ, θ_0	=	azimuthal angle (as in Eq. (1))
ϕ	=	phase angle (as in Eq. (1))

II. Introduction

Deep axisymmetric cavities are an interesting topic in fluid dynamics and aeroacoustics because of their rich modal behavior and their relevance to both real-world engineering applications and fundamental phenomena. Such cavities can exhibit interactions between shear layer instabilities and trapped acoustic modes, which form a feedback loop that causes self-sustained oscillations and symmetry-breaking phenomena. The study of these phenomena allows us to better understand the flow-acoustic coupling mechanisms, which have practical implications *e.g.,* in turbomachinery noise control, combustion chamber design, as well as landing-gear noise[1–4]. Foundational works, such as[5,6], and relatively more recent contributions, like[7,8], have laid the groundwork for this field. Recent advances reveal intricate dynamics, such as induced mean flow swirl[9,10], and demonstrate how subtle changes in geometry can significantly affect aeroacoustic responses[11].

In the works of Faure-Beaulieu et al.[9,10], the authors present an experimental investigation of acoustic modes in a deep axisymmetric cavity within a turbulent pipe flow. They demonstrate the possibility of obtaining a strong feedback loop between hydrodynamic and acoustic modes, with amplitudes of up to about 10 kPa. They observe different regimes in which the phenomenon occurs, referred to as a pure spinning, a beating, and a mixed regime. It is also demonstrated that when the system maintains a spinning state for a sustained period, this can induce a swirl in the mean flow, breaking the axisymmetry. This mean swirl is shown to favor the spinning state, which is further investigated by imposing a mean swirl at the inflow.

*Assistant professor, Faculty of Aerospace Engineering, Department of Flow Physics and Technology, f.deprenter@tudelft.nl.
†Full professor, Faculty of Aerospace Engineering, Department of Flow Physics and Technology, d.casalino@tudelft.nl.

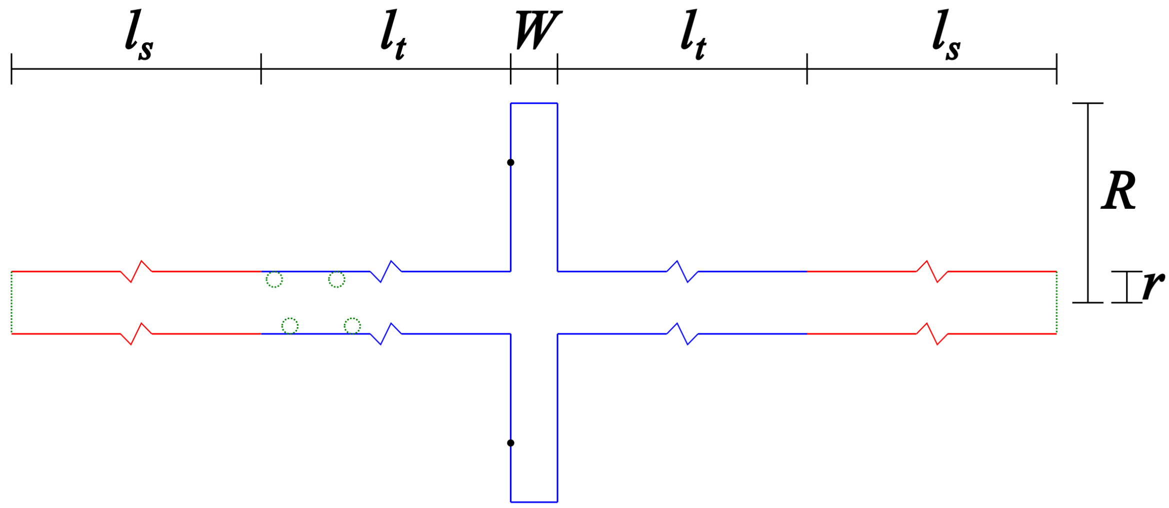

Figure 1. Sketch of the axisymmetric geometry. Red lines indicate frictionless walls in the sponge, blue lines no-slip walls, and dashed green lines inlets and outlets.

In this contribution, we first numerically corroborate the behavior of the system, including *i)* the different coupled hydrodynamic-acoustic modes and regimes, *ii)* the swirling of the mean flow caused by the spinning state, and *iii)* the effect of imposing a mean swirl at the inflow. Second, we investigate the effect of minor geometric modifications, which are straightforward in a numerical study but would be challenging to achieve experimentally. Specifically, we introduce a slight asymmetry in the cavity in the range of 0.1–0.6%. As demonstrated by the results, this asymmetry affects the regime of the feedback mechanism and influences the beating frequency in the corresponding regime. Additionally, the numerical study captures three-dimensional fields, which enables to investigate turbulent structures.

This document is structured as follows. In Sec. III we describe the numerical setup, boundary conditions, and outputs. Sec. IV describes the formulation of the acoustic modes in the cavity, which we employ to identify the different regimes. Sec. V presents the results, including the corroboration of experimental measurements, flow visualizations, and the investigation of variations in geometry. Finally, Sec. VI summarizes the work and provides concluding remarks.

III. Geometry and numerical model

The simulated geometry of a pipe flow with a deep axisymmetric cavity is illustrated in Fig. 1. Along the axis, it consists of five sections: *i)* a long frictionless tube of radius $r = 20\,\mathrm{mm}$ and length $l_s = 26\,\mathrm{m}$ that acts as an acoustic sponge, *ii)* a tube of the same radius r and length $l_t = 769\,\mathrm{mm}$ with a no-slip boundary condition that allows for the development of a turbulent pipe flow, *iii)* the axisymmetric cavity with radius $R = 128\,\mathrm{mm}$ and width $W = 30\,\mathrm{mm}$, *iv)* another no-slip tube of the same dimensions, and *v)* another frictionless tube that acts as an acoustic sponge. Note that, except for the sponges, this matches the geometry in Ref.[9].

To investigate minor geometric variations, we break the axisymmetry by scaling the cavity depth. As indicated in the left panel of Fig. 2, the vertical and out-of-plane directions (w.r.t. Fig. 1) are scaled by α and $1/\alpha$, respectively. Note that this involves only small modifications, *i.e.,* $1 \leq \alpha \leq 1.0063$. We discuss the intended effect of this scaling at the end of Sec. IV.

Multiple inflows are illustrated in Fig. 1. The primary inflow is at the end of the sponge on the left side of the figure. Another set of four circular inflows is sketched at the start of the physical (*i.e.,* no-slip) part of the tube, hereafter referred to as swirl inflows. These inflows are employed to impose a mean swirl, which affects the dominant state of the system. The swirl inflows have a radius of 5 mm and are placed respectively 15 mm, 25 mm, 55 mm, and 65 mm from the start of the physical tube. The swirl inflows are also illustrated on the right of Fig. 2. In all cases, the massflow through the primary inflow is corrected for the swirl inflows,

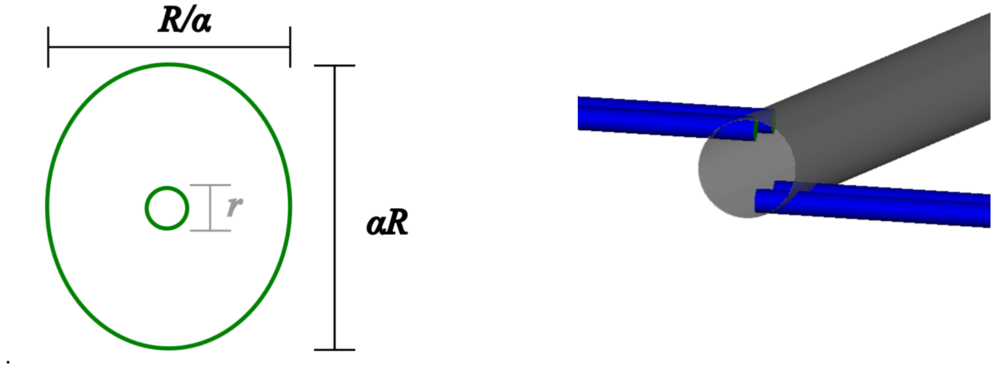

Figure 2. Left: geometrical variation in the cavity that breaks the axisymmetry through scaling parameter α (the figure is exaggerated for visualization). Right: close-up of the swirl inflows (transparent gray the physical tube; blue the swirl inflow tubes; green the actual swirl inflow inlets).

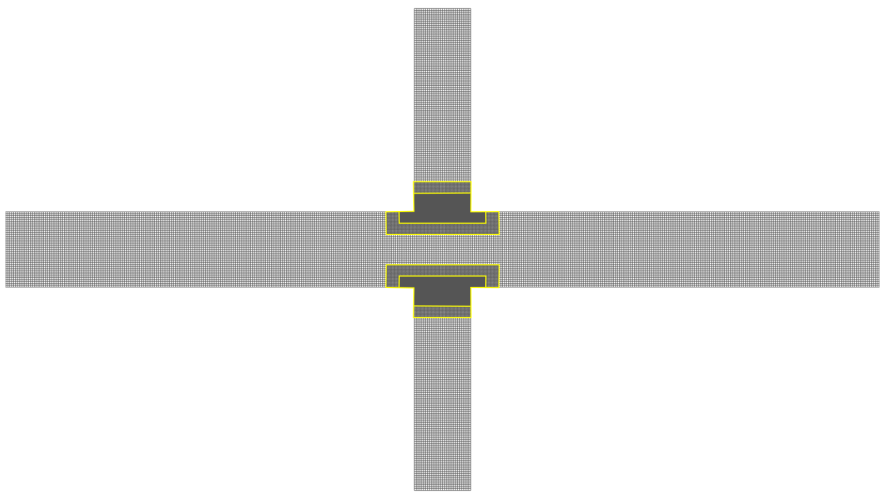

Figure 3. Distribution of the VR regions in the vicinity of the cavity. The regions correspond to a voxel sizes of respectively 0.25 mm, 0.5 mm and 1.0 mm.

such that the total inflow equals either 33.5 g/s or 67 g/s, resulting in a mean flow velocity in the tube of 23.5 m/s or 47 m/s. At the downstream end of the geometry in Fig. 1, there is an outflow condition with pressure 95 300 Pa. Additional physical constants are set to a temperature of 293 K, a kinematic viscosity of 15.1 mm^2/s, and a speed of sound of $c = 343$ m/s.

The simulation is performed with the low-subsonic model of the high-fidelity Lattice Boltzmann Very Large Eddy Simulation (LBM-VLES) solver PowerFLOW® 6-2025-R2. The model employs ten Variable Resolution (VR) regions. The three finest regions with mesh sizes ranging from 0.25 mm to 1.0 mm a re employed in the physical part of the domain with no-slip conditions (blue lines in Fig. 1) and are distributed as illustrated in Fig. 3. The sponge region employs an additional seven VR regions in the frictionless tube (red lines in Fig. 1), with a mesh size up to 128 mm. In this sponge, the (dimensionless) grid bulk viscosity increases linearly to 0.5 over a length of 200 mm, after which the grid is sequentially coarsened to attenuate all frequencies above approximately 100 Hz. The model comprises 9.4 million voxels, of which 0.24 million are located in the sponge. The simulation takes approximately 6 kCPU hours per physical second.

For all scenarios, the simulation is first run for 1 s of physical time for initialization. This corresponds to approximately 30 flow-through times of the physical tubes and 800 periods of the primary acoustic cycle. After the initialization, pressure signals are sampled at a frequency of 28 kHz using 36 virtual microphones in the left wall of the cavity (*i.e.,* inlet side), evenly distributed in the azimuthal direction at a radius of 90 mm, illustrated by the black dots in Fig. 1. The simulations run for a total physical time of 5 s. During the

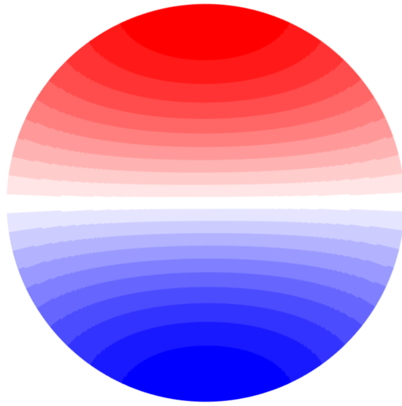

Figure 4. First-order azimuthal and zero-order radial mode.

last 0.25 s, a volumetric field in the neighborhood of the cavity is stored at a frequency of 15 kHz, capturing approximately 200 acoustic cycles with 20 frames per cycle.

IV. Acoustic modes

In this section, we present the relevant acoustic modes in the deep cavity and the parameters used to describe these modes. The motivation for the previously defined parameter α, as well as its intended effect, is explained based on these modes.

As discussed in detail in Ref.[9], the most important acoustic mode in the cavity is the first-order azimuthal mode with zero radial order[12,13]. Its mode shape is illustrated in Fig. 4 and is given by $J_1(\beta_{10}r/R)\sin(\theta-\theta_0)$, with r and θ the radial and azimuthal coordinates, $J_1(\cdot)$ the first-order Bessel function of the first kind, $\beta_{10}=1.84$ is the first root of $J_1'(\cdot)$, R the outer radius, and θ_0 defines the azimuthal orientation. The mode has a frequency of $f_{10}=c\beta_{10}/2\pi R\approx 785\,\text{Hz}$. In a perfectly cylindrical environment, it forms a pair of degenerate eigenvalues, which may manifest itself as a standing mode (*i.e.,* $p\propto J_1(\beta_{10}r/R)\sin(\theta-\theta_0)\sin(\omega t)$), as a spinning mode (*i.e.,* $p\propto J_1(\beta_{10}r/R)\sin(\theta-\theta_0\pm\omega t)$), or as a combination of these.

To describe the nature (*i.e.,* standing or spinning) of the acoustic perturbation, we employ the quaternion notation introduced in Ref.[14]. At a given radius, the pressure is defined as:

$$p(\theta,t)=A(t)\left(\,\cos(\chi(t))\,\cos(\theta-\theta_0(t))\,\cos(\omega t+\phi(t))\;+\;\sin(\chi(t))\,\sin(\theta-\theta_0(t))\,\sin(\omega t+\phi(t))\,\right). \quad (1)$$

In this equation, $A(t)$, $\chi(t)$, $\theta_0(t)$, and $\phi(t)$ denote slowly varying variables that vary on timescales much longer than the wave period. $0<A(t)$ denotes the amplitude in Pa; $-\pi/4\leq\chi(t)\leq\pi/4$ defines the nature angle, with $\chi(t)=\pm\pi/4$ a left/right pure spinning state, $\chi(t)=0$ a pure standing state, and with intermediate values corresponding to a combination of these; $-\pi/2\leq\theta_0(t)\leq\pi/2$ the azimuthal orientation of the standing component; and $-\pi\leq\phi(t)\leq\pi$ the phase. These slowly varying variables are extracted from the pressure sampled at the virtual microphones by the following procedure:

1. The data for each microphone is split into segments of 36 sampling points, which is the integer number closest to the natural wave period.

2. For each segment the data of all microphones is projected onto four harmonic basis functions: $g_1(\theta,t)=\cos(\theta)\cos(2\pi f_{10}t)$, $g_2(\theta,t)=\cos(\theta)\sin(2\pi f_{10}t)$, $g_3(\theta,t)=\sin(\theta)\cos(2\pi f_{10}t)$, $g_4(\theta,t)=\sin(\theta)\sin(2\pi f_{10}t)$. This results in the respective coefficients b_1, b_2, b_3, and b_4.

3. A, χ, θ_0, and ϕ are calculated using Algorithm 1. The projection onto these variables becomes singular if $\chi(t)\approx\pm\pi/4$. Therefore, we set $\theta_0=0$ in case $|\sin(2\chi)|\geq 0.999$.

Algorithm 1 Extract A, χ, θ_0, and ϕ

$A = \sqrt{b_1^2 + b_2^2 + b_3^2 + b_4^2}$
$\chi = \frac{1}{2}\arcsin\left(\frac{2\,(b_1 b_4 - b_2 b_3)}{A^2}\right)$
if $|\sin(2\chi)| \geq 0.999$ **then**
  $\theta_0 = 0$
  $\phi = \mathrm{atan2}\left(-\frac{b_2}{A\cos\chi}, \frac{b_1}{A\cos\chi}\right)$
else
  $c_1 = \frac{b_1\cos(\chi) - b_4\sin(\chi)}{A\cos(2\chi)}$
  $c_2 = \frac{-b_4\cos(\chi) + b_1\sin(\chi)}{A\cos(2\chi)}$
  $c_3 = \frac{-b_2\cos(\chi) - b_3\sin(\chi)}{A\cos(2\chi)}$
  $c_4 = \frac{b_3\cos(\chi) + b_2\sin(\chi)}{A\cos(2\chi)}$
  if $|c_1| > |c_3|$ **then**
    $\theta_0 = \arctan\left(\frac{c_4}{c_1}\right)$
  else
    $\theta_0 = \arctan\left(\frac{c_2}{c_3}\right)$
  end if
  if $|c_1| > |c_4|$ **then**
    $\phi = \mathrm{atan2}\left(\frac{c_3}{\cos\theta_0}, \frac{c_1}{\cos\theta_0}\right)$
  else
    $\phi = \mathrm{atan2}\left(\frac{c_2}{\sin\theta_0}, \frac{c_4}{\sin\theta_0}\right)$
  end if
end if

As described in Sec. III, we have introduced a parameter $1 \leq \alpha \leq 1.0063$ to create a slight asymmetry in the geometry. Because of this geometric modification, the degenerate eigenvalue pair separates into two very close eigenvalues: a horizontal and a vertical standing mode with frequencies of approximately $f_{10}\alpha$ and f_{10}/α, respectively. Assuming that the flow does not strongly perturb these natural eigenmodes, the modes will oscillate independently at their own natural frequency and go in and out of phase with each other approximately every $\alpha/(\alpha^2-1)$ oscillations, equivalent to a frequency of approximately $\alpha f_{10}/(\alpha^2-1)$. A numerical eigenvalue analysis provides similar values, with a beating frequency of $1.84 f_{10}(\alpha-1)$ or $0.54/(\alpha-1)$ natural periods. When both modes have the same amplitude, this means the system will alternate between two states: *i)* For a period of time there will be a left/right spinning state during which the modes have a phase difference of approximately $\pm\pi/2$ to each other. *ii)* When one mode catches up with the other, there will at some point be a phase difference of 0 or π between the modes. This results in a standing state with $\theta_0 = \pm\pi/4$, *i.e.,* with the nodes and antinodes on the diagonals at 45° with the horizontal/vertical axes. The alternation between spinning and standing is referred to as the beating regime. As will be demonstrated in Sec. V, the feedback loop through the hydrodynamic modes is stronger in the pure spinning regime. Therefore, geometries with minor levels of asymmetry still behave in the spinning regime. With larger values of α, the two separate natural eigenfrequencies become more distinct, and a beating regime prevails. By simulating geometrical variations that deviate from perfect axisymmetry at different levels, we intend to determine the sensitivity of the coupled system to imperfections in the geometry. Furthermore, we investigate how a mean swirl imposed at the inflow affects the value of α at which the system transitions from pure spinning to beating. This final investigation is based on the observation that a mean swirl affects the strength of the feedback loops in favor of a pure spinning regime.

V. Results

In this section, we first discuss a perfectly axisymmetric case without an imposed mean swirl at the inflow. We then show the effect of small imperfections in the axisymmetry of the geometry. Finally, we demonstrate the effect of imposing a mean swirl at the inflow.

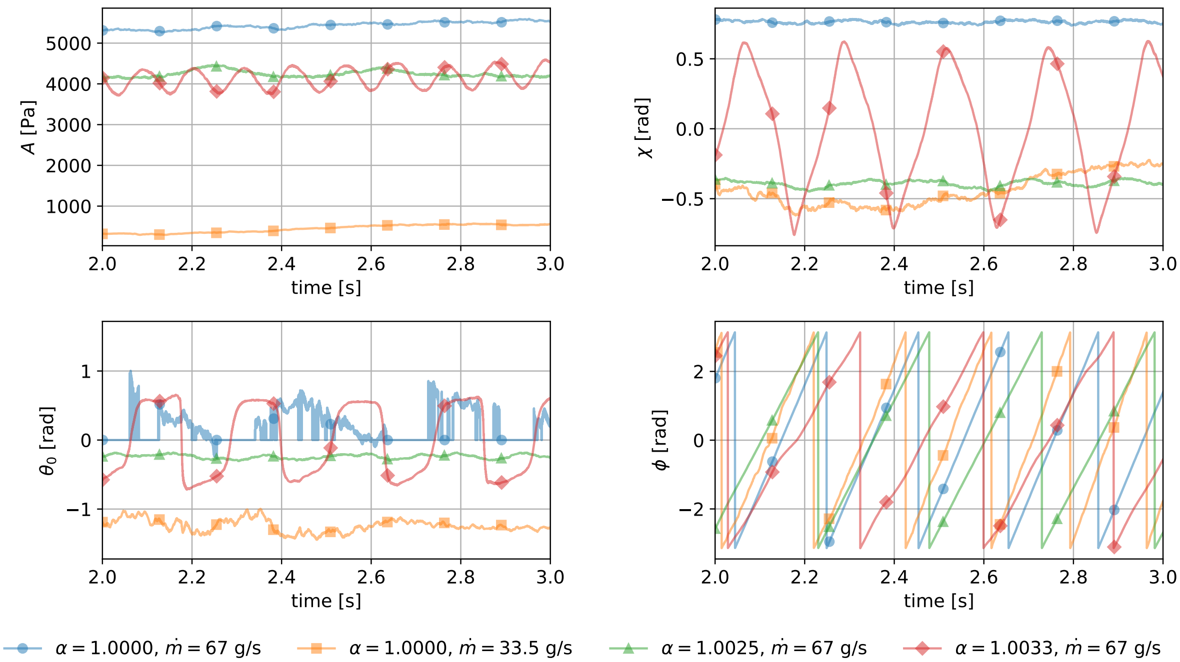

Figure 5. Slowly varying variables over time for selected cases with no imposed mean swirl at the inflow.

The slowly varying variables for a perfect axisymmetric case without an imposed mean swirl are plotted in blue and yellow in Fig. 5. The blue line represents the case with a massflow of 67 g/s, which corresponds to a mean velocity in the tube of 47 m/s. The convection time for turbulent structures through the shear layer of the cavity at this velocity approximately matches the natural period of the acoustic mode, forming a strong hydrodynamic-acoustic feedback loop. A pure spinning regime prevails during the entire simulation, following from the very steady nature angle $\chi \approx \pi/4$ and amplitude $A \approx 5.5\,\mathrm{kPa}$, which is close to what was observed experimentally in Ref.[9]. Due to the pure spinning regime, the orientation angle does not provide much meaningful information, and in fact is forced to zero for most of the timesteps since the projection becomes singular when χ gets too close to $\pi/4$. The linear trend in the phase ϕ is caused by a mismatch in the approximated and actual frequency. The hydrodynamic structures in this interaction are visualized by a λ_2 isosurface in the top row of Fig. 6. The spinning acoustic mode initiates the shedding of a vortex at the upstream edge of the cavity. This vortex is convected downstream, forming a single helix. The yellow line in Fig. 5 corresponds to exactly half of the massflow and mean velocity, *i.e.,* 33.5 g/s and 23.5 m/s. Consequently, the convection time through the shear layer is approximately twice the acoustic period. Also in this case, the spinning mode is predominant, although less so than at the higher massflow. This is visible in the lower amplitude of approximately $A \approx 0.5$ kPa and a less consistent nature angle of $-0.6 \lesssim \chi \lesssim -0.3$. Note that without an imposed mean swirl at the inflow, the spinning direction is stochastic. While also Ref.[9] mentioned a stronger feedback loop with the higher velocity experimentally, it should be mentioned that we have not investigated small variations in the massflow. Therefore, it is possible that the higher massflow of 67 g/s is closer to a local maximum in the amplitude than the lower massflow of 33.5 g/s. The second row of Fig. 6 shows the λ_2 visualization of the turbulent structures, obtained at $t = 2.25$ s where $\chi \approx -0.6$ was obtained. By the same mechanism as at the higher velocity, the lower velocity forms an approximately double helix.

A slight asymmetry of 0.25% (*i.e.,* $\alpha = 1.0025$) with the higher massflow of 67 g/s significantly alters the system behavior. The green line in Fig. 5 shows that the amplitude is reduced to $4.2\,\mathrm{kPa}$. The nature angle $\chi \approx -0.4$ indicates a steady mixed regime, combining aspects of both a spinning and a standing mode, with maximum pressures in the (spinning and standing) antinodes of $1.6\,\mathrm{kPa}$ and $2.2\,\mathrm{kPa}$, respectively. It is interesting that the sum of these yields a maximum pressure amplitude in the antinodes of the standing mode of $3.9\,\mathrm{kPa}$, which is equal to the antinodal pressure of $5.5/\sqrt{2} = 3.9\,\mathrm{kPa}$ in the pure spinning regime

$\alpha = 1.0000$
$\dot{m} = 67$ g/s

$\alpha = 1.0000$
$\dot{m} = 33.5$ g/s

$\alpha = 1.0025$
$\dot{m} = 67$ g/s

$\alpha = 1.0033$
$\dot{m} = 67$ g/s

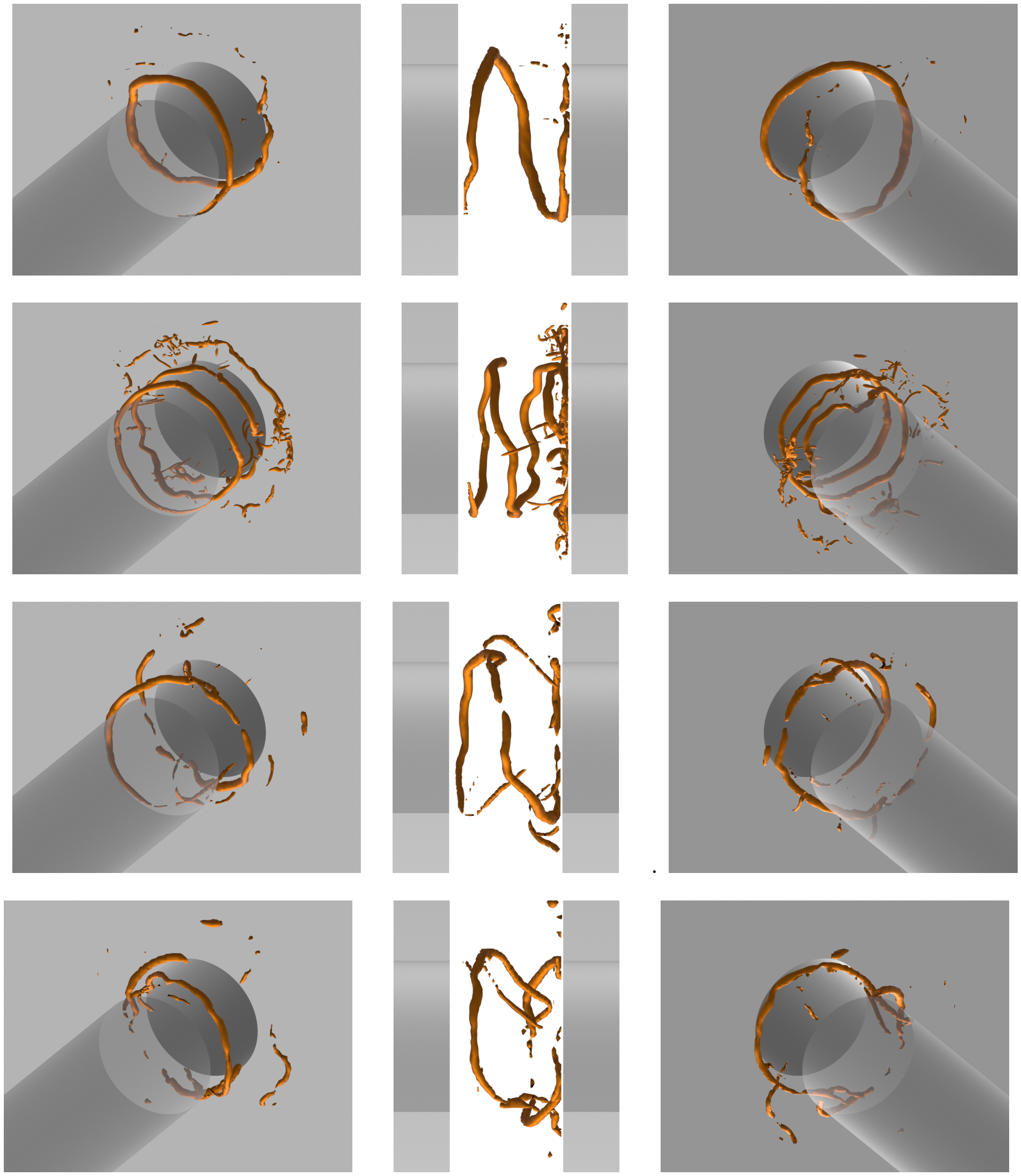

Figure 6. Vortical structures for selected cases visualized by $\lambda_2 \in \{-3 \cdot 10^{-7}, -2 \cdot 10^{-8}\}$ s^{-2} isosurfaces for $\dot{m} \in \{33.5, 67\}$ g/s. Left, middle, and right figures are from viewpoints upstream, to the side, and downstream of the cavity.

for the perfectly symmetric case. The orientation angle θ_0 is relatively steady around -0.23 rad. This could indicate that the depth (and consequently the frequency of a standing wave) of the cavity in that direction provides the strongest feedback loop. The latter is supported by the fact that simulations with $\alpha \in \{1.0016, 1.0020, 1.0024, 1.0026\}$ resulted in (absolute) mean orientation angles $\theta_0 \in \{\approx 0.34, \approx 0.26, \approx 0.24, \approx 0.23\}$ rad, respectively. The phase ϕ is very close to the previously discussed cases, with a slightly different slope indicating a small change in frequency. The hydrodynamic structures are visualized in the third row of Fig. 6. It can be seen that the spinning mode remains predominant, with a (weaker) additional vortex generated by the standing mode.

Further increasing the asymmetry increases the difference between the two separate standing modes' eigenfrequencies. Consequently, the natural beating behavior of the acoustic system outweighs the strength of the spinning feedback loop. For an asymmetry level of 0.33% (*i.e.,* $\alpha = 1.0033$), the slowly varying variables are shown in red in Fig. 5. The results show that the nature angle χ varies almost linearly between

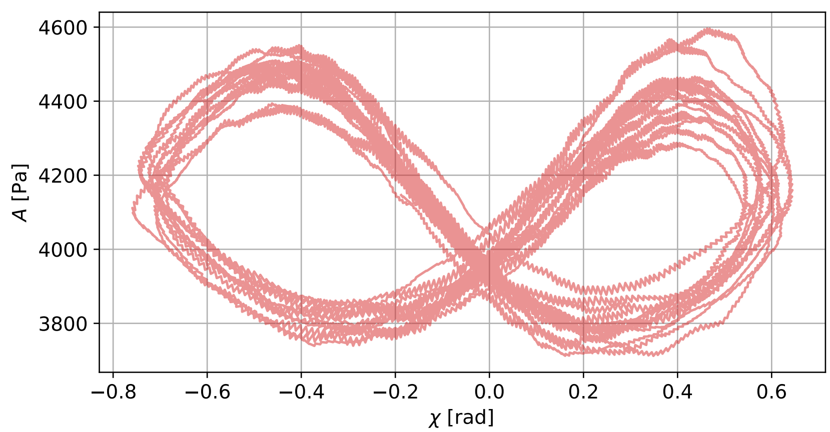

Figure 7. Amplitude A plotted against nature angle χ for $\alpha = 1.0033$.

$\pi/4$ and $-\pi/4$. This describes a constant change from a (left) spinning state at $\chi \approx \pi/4$, to a standing state at $\chi \approx 0$, to a (right) spinning state at $\chi \approx -\pi/4$, to a standing state again at $\chi \approx 0$, and back to a (left) spinning state. The beating frequency of the system is discussed at the end of this section in Fig. 10. The amplitude A shows a small oscillation at double the beating frequency, indicating a stronger feedback loop for the spinning mode. This is further illustrated in Fig. 7. In this figure, the amplitude is plotted against the nature angle, and it is evident that the amplitude grows for $|\chi| \gtrsim 0.4$ and decreases for $|\chi| \lesssim 0.4$. The orientation angle continuously alternates between $\theta_0 = \pi/4$ and $\theta_0 = -\pi/4$. This is because the geometry modification through α (Fig. 2(a)) causes a separate horizontal and vertical standing mode. As discussed in Sec. IV, when these are in-phase or in antiphase, the sum of these forms an acoustic mode with the nodes and antinodes on the diagonals. The phase ϕ is overall similar to the previously presented results. The gentler slope that accumulates to slightly more than 2π of difference with the other cases, shows the system's frequency is approximately 1 Hz lower. The slight deviations from a straight line indicate that the frequency during the spinning phase of the beating motion is slightly different from the frequency during the standing phase. The hydrodynamic structures that are shed during the standing phase are visualized by a λ_2 isosurface in the fourth row of Fig. 6. It is visible that U-shaped vortices are shed sequentially from opposite sides of the cavity's upstream edge.

Ref.[9] concluded that a spinning state for a sustained period of time causes a mean swirl in the flow, which in turn promotes the spinning state. On this basis, the effect of imposing a mean swirl at the inflow is investigated. This is also numerically replicated, with massflows of 4.5 g/s and 9 g/s through the the combined swirl inflows. The flow through the primary inflow is corrected to maintain the total massflow at 67 g/s. To compare the strength of a self-induced mean swirl with that of a mean swirl imposed at the inflow, both cases are displayed in Fig. 8. The effect of the imposed mean swirl is reported in Fig. 9. The top panel shows the resulting range of amplitudes A for the different swirl massflows and for different levels of asymmetry. For all swirl massflows, the results show an initially narrow range of amplitudes that decreases with α, until α reaches the threshold for the beating regime and the range of amplitudes widens. The bottom panel shows the resulting range of the nature angle χ for the same systems. Similarly, all swirl massflows initially show a narrow range, which for smaller values of α is dominated by a pure spinning regime. With increasing α a larger standing component develops (*i.e.,* χ closer to 0) forming a mixed regime. The range of χ widens for values of α beyond the threshold of the beating regime, and it can be observed that with an imposed swirl the beating is no longer symmetric. While an effect of the swirl massflow on the required level of asymmetry to obtain a beating regime was anticipated, it is surprising that the required level of asymmetry is larger for a swirl massflow of 4.5 g/s than for a swirl massflow of 9 g/s. We hypothesize that this can be explained by the phase angle between a spinning acoustic mode and the vortex impingement at the downstream edge of the cavity. With a mean swirl, the vortex that is initiated at the upstream edge of the cavity by the spinning acoustic mode is not only convected axially through the shear layer but also azimuthally. Therefore, the mean swirl affects the phase angle between the impingement of the helical vortex and the acoustic mode, which explains how the strength of the feedback loop depends on the mean swirl of the flow. This suggests that the amount of mean swirl at which the strongest feedback loop and the highest

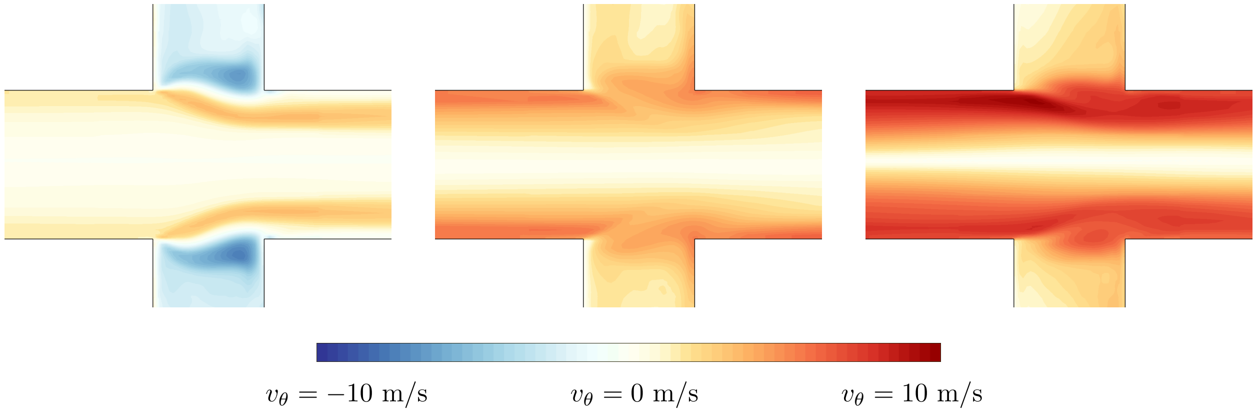

Figure 8. Mean tangential velocity fields in the cavity. Left: the self-induced mean swirl from the hydrodynamic-acoustic feedback loop for the perfectly symmetric case ($\alpha = 1.0000$). Middle: mean swirl imposed at the inflow with a swirl massflow of 4.5 g/s for the case of $\alpha = 1.0063$. Right: mean swirl imposed at the inflow with a swirl massflow of 9 g/s for the case of $\alpha = 1.0039$. For the middle and right panels, the values of α were chosen to ensure a beating regime. This isolates the effect of the inflow-imposed swirl, without contributions from the self-induced mean swirl associated with a pure spinning regime.

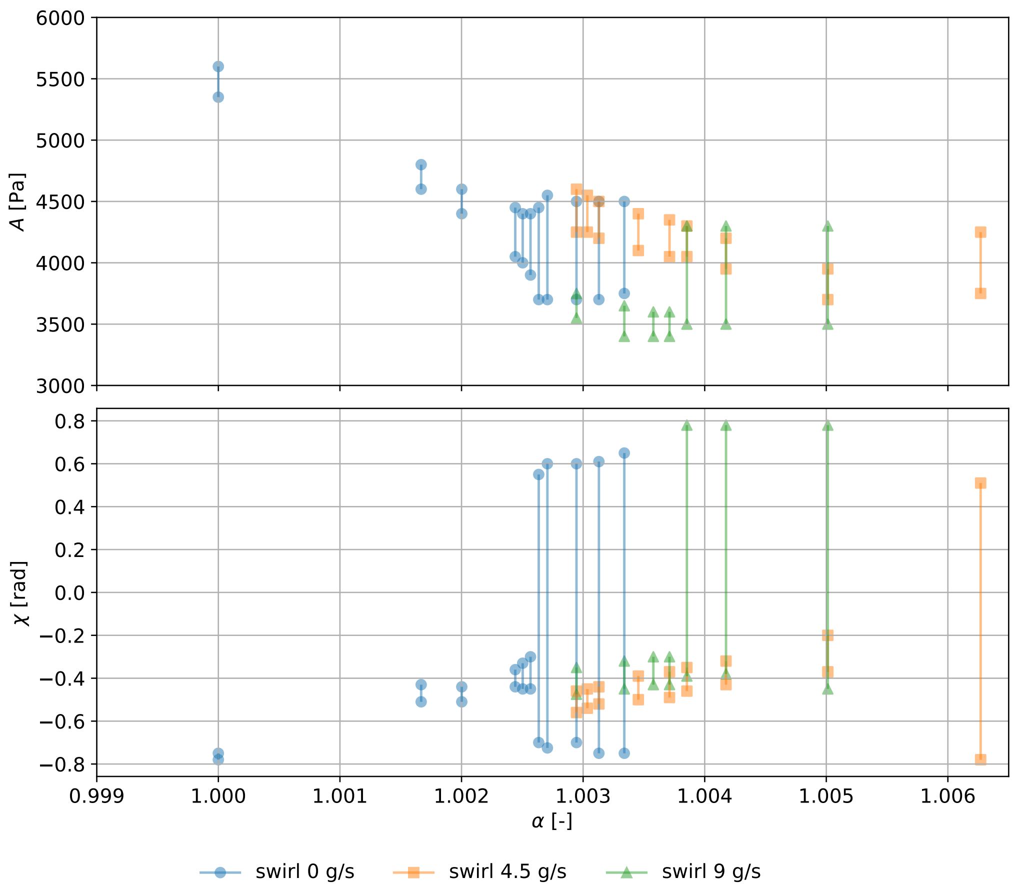

Figure 9. Observed ranges of amplitude A and nature angle χ for the different swirl massflows plotted against the level of asymmetry α. As the rotation direction in a pure spinning regime without imposed mean swirl is stochastic, positive values of χ for non-beating cases have been inverted to enhance readability.

amplitude is obtained will be dependent on the convection time through the shear layer. Consequently, we expect that the specific response to mean swirl is sensitive to the axial velocity (or total massflow) of the system. In this regard, it should be mentioned that the asymmetry of the beating motion in the nature angle χ in Fig. 9 is also opposite for the massflows of 4.5 and 9 g/s. This indicates that the different swirl massflows obtain the strongest feedback loop in the spinning mode at opposite spinning directions.

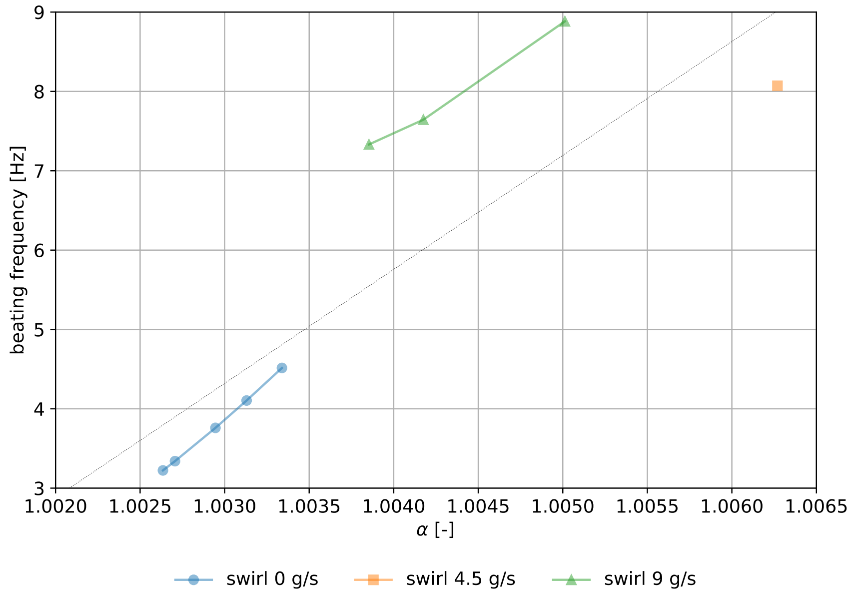

Figure 10. Beating frequency plotted against the level of asymmetry α. The dashed line represents the difference between the smallest two purely acoustic eigenvalues, which corresponds to the beating frequency in the absence of flow-acoustic interaction.

Finally, we investigate the beating frequency for systems in a beating regime. Fig. 10 plots the resulting beating frequencies against the level of asymmetry. As one would expect, the beating frequency increases with the level of asymmetry. The results also indicate a strong effect of the mean swirl on the beating frequency, and a significant difference between the purely acoustic (dashed line) predictions and the resulting frequencies from the coupled hydrodynamic-acoustic system. While the results were obtained with different levels of asymmetry, the obtained frequencies with a swirl massflow of 4.5 g/s seem lower than without an imposed swirl, while the frequencies obtained with a swirl massflow of 9 g/s are higher. Also this observation can possibly be correlated to the asymmetry in the beating motion, with the dominant spinning direction either aligned to or opposite to the swirl.

VI. Concluding remarks

This manuscript presents numerical simulations of an aeroacoustic instability in a quasi-axisymmetric cavity that replicates previously published experimental studies[9,10]. The results corroborate experimental findings and demonstrate that the behavior of the system, *i.e.,* pure spinning versus beating regimes, strongly depends on the level of asymmetry. For small levels of asymmetry, the spinning regime is favored, which provides the strongest feedback loop. For higher levels of asymmetry the beating regime prevails. The effect of imposing a mean swirl is also investigated. While the mean swirl promotes the spinning regime in all presented results, the evaluation also suggest that the effect of a mean swirl will strongly depend on the total massflow. A topic for future research is to investigate how variations in the mean swirl and the total massflow affect stable flow structures using resolvent analysis. We expect that this will enable specification of the correlation between these parameters and the strength of the feedback loops, and consequently the dominant regime.

Acknowledgments

The computations in this work used the Dutch national e-infrastructure with the support of the SURF Cooperative using grant no. EINF-15704. The research of Frits de Prenter is supported by the NWO Veni scheme grant no. 20153 (STABILIZE).

References

[1] Moreau, S. and Roger, M., "Turbomachinery Noise Review," *International Journal of Turbomachinery Propulsion and Power*, Vol. 9, 2024, pp. 11.

[2] Blondé, A., Pandey, K., Schuermans, B., and Noiray, N., "Intrinsic aeroacoustic instabilities in the crosstalk apertures of can-annular combustors," *arXiv preprint*, 2024.

[3] Casalino, D., Ribeiro, A. F., and Fares, E., "Facing rim cavities fluctuation modes," *Journal of Sound and Vibration*, Vol. 333, No. 13, 2014, pp. 2812–2830.

[4] Casalino, D., Ribeiro, A. F. P., Fares, E., and Nölting, S., "Lattice-Boltzmann Aeroacoustic Analysis of the LAGOON Landing Gear Configuration," *AIAA Journal*, Vol. 52, No. 6, 2014, pp. 1232–1248.

[5] East, L., "Aerodynamically induced resonance in rectangular cavities," *Journal of Sound and Vibration*, Vol. 3, No. 3, 1966, pp. 277–287.

[6] Rockwell, D. and Naudascher, E., "Self-sustaining oscillations of flow past cavities," *Journal of Fluids Engineering*, Vol. 100, No. 2, 1978, pp. 152–165.

[7] Aly, K. and Ziada, S., "Flow-excited resonances of trapped modes of ducted shallow cavities," *Journal of Fluids and Structures*, Vol. 26, No. 1, 2010, pp. 92–120.

[8] Aly, K. and Ziada, S., "Azimuthal behaviour of flow-excited diametral modes of internal shallow cavities," *Journal of Sound and Vibration*, Vol. 330, No. 15, 2011, pp. 3666–3683.

[9] Faure-Beaulieu, A., Xiong, Y., Pedergnana, T., and Noiray, N., "Self-sustained azimuthal aeroacoustic modes. Part 1. Symmetry breaking of the mean flow by spinning waves," *Journal of Fluid Mechanics*, Vol. 971, 2023, pp. A21.

[10] Faure-Beaulieu, A., Pedergnana, T., and Noiray, N., "Self-sustained azimuthal aeroacoustic modes. Part 2. Effect of a swirling mean flow on the modal dynamics," *Journal of Fluid Mechanics*, Vol. 971, 2023, pp. A22.

[11] Ho, Y. and Kim, J., "A wall-resolved large-eddy simulation of deep cavity flow in acoustic resonance," *Journal of Fluid Mechanics*, Vol. 917, 2025, pp. A17.

[12] Rienstra, S. W., "A classification of duct modes based on surface waves," *Wave Motion*, Vol. 37, No. 2, 2003, pp. 119–135.

[13] Morse, P. M. and Ingard, K., *Theoretical Acoustics*, McGraw-Hill, New York, 1968.

[14] Ghirardo, G. and Bothien, M. R., "Quaternion structure of azimuthal instabilities," *Phys. Rev. Fluids*, Vol. 3, 2018, pp. 113202.